J. Fluid Mech. (1995), *vol.* 291, *pp.* 299–322

The evolution of the coherent structures in a uniformly distorted plane turbulent wake

By G. A. KOPP, J. G. KAWALL AND J. F. KEFFER
Department of Mechanical Engineering, University of Toronto, Toronto, Canada, M5S 1A4

(Received 22 March 1994 and in revised form 28 November 1994)

A plane turbulent wake generated by a flat plate is subjected to a uniform distortion. It is observed that nearly two-dimensional, quasi-periodic coherent structures dominate the distorted wake. Rapid distortion theory, applied to a kinematic vortex model of the coherent structures in the undistorted far wake, predicts many of the effects revealed by a hot-wire anemometry/pattern-recognition analysis of these structures. Specifically, rapid distortion theory predicts reasonably well the observed changes in the ensemble-averaged velocity patterns and the disproportionate amplification of the large-scale coherent structures relative to the smaller-scale 'isotropic' eddies. These results are consistent with the view that self-preservation of the distorted wake is not possible because of the selective amplification of the coherent structures, which control the development of the wake. As well, the entrainment rate in the distorted wake increases at a rate greater than that predicted by the self-preservation theory.

1. Introduction

Vortex stretching is known to be an important mechanism in turbulent shear flows. However, determining the effect of the mean strain field caused by a shear flow on the turbulent eddies, both large and small, is not a straightforward matter. Imposing a prescribed strain on a turbulent flow can shed new structural information on turbulent eddies and coherent structures and thus lead to further insight into mixing, entrainment, and self-preservation of the flow. To this end, distorting ducts have been used to apply mean rates of strain to various turbulent flows (e.g. Townsend 1954; Reynolds 1962; Keffer 1965; Tucker & Reynolds 1968; Keffer *et al.* 1978; Townsend 1980; Elliot & Townsend 1981; Kawall & Keffer 1982; Kopp, Kawall & Keffer 1995).

Taylor (1935) was the first to calculate the effect of straining turbulent eddies by applying what has become known as rapid distortion theory (RDT) to an array of eddies (of a given size) passing through a wind tunnel contraction. Batchelor & Proudman (1954) improved the basic RDT by including all eddy sizes present in a turbulent spectrum and established the conditions necessary for the validity of RDT.

Townsend's (1954) uniformly distorted grid turbulence experiments showed reasonable agreement with Batchelor & Proudman's RDT. Specifically, based on a peak appearing in the energy spectrum, Townsend's experimental results implied that selective amplification of the large eddies occurred. Keffer's (1965) flow visualization of a uniformly distorted turbulent wake suggested that the large eddies (with spanwise vorticity) in the far field of a cylinder-generated wake were progressively amplified by the imposed mean rate of strain and, thus, eventually dominated the flow. Kawall & Keffer's (1982) experimental analysis of the intermittent turbulent bulges of the distorted wake confirmed that the large eddies grew in the lateral direction as the wake

evolved within the distortion, in spite of the fact that the characteristic (lateral) lengthscale of the flow decreased. Kopp *et al.* (1995) applied Taylor's basic RDT to a preliminary kinematic model of the far-wake coherent structures, with good qualitative success in terms of the agreement between the predicted results and the pattern-recognition (PR) results obtained experimentally with a rake of normal wires. Not only did they predict with reasonable accuracy the change in size of the structures, they also predicted the change in the mean-velocity lengthscale. It should be noted that the more complicated RDT due to Hunt & Mulhearn (1973) was used by Keffer *et al.* (1978) to predict the change in the thermal lengthscale of a uniformly distorted heated mixing layer. The degree of success of this prediction was much the same as that with which Kopp *et al.* (1995) predicted the velocity lengthscale in their distorted turbulent wake.

In the present work, a rake of X-wires is used in conjunction with the PR technique to examine the detailed features of both the spanwise and lateral coherent structures of a uniformly distorted plane turbulent wake. The results show that far-wake coherent structures become significantly two-dimensional and quasi-periodic; indeed, a type of Kármán vortex street starts appearing. However, the structures within this quasi-Kármán vortex street are basically different from the Kármán-like vortices present in the near wake. The fundamental changes in the coherent structures due to the distortion field would suggest that the distorted wake does not become self-preserving. The kinematic model of Kopp *et al.* (1995) is refined and used in conjunction with Taylor's RDT to shed further light on the development of the coherent structures in the distorting duct.

2. Experimental details

A flat plate, mounted vertically and parallel to the z-axis, the spanwise axis (see figure 1), was used to generate a plane turbulent wake in an open circuit, variable-speed wind tunnel containing a distortion section (see figure 2). A definition sketch of the wake is presented in figure 1, where U_0 is the free-stream velocity, l_0 is the mean-velocity half-width lengthscale, and W is the width of the flat plate. Upstream of the distorting duct, the test section has nominal dimensions of 23 cm wide by 46 cm high. The distortion section has exponentially varying sides, with a constant cross-sectional area, and applies a uniform irrotational strain to the flow. With the mean streamlines following the exponentially varying tunnels walls, the strain ratio components are as follows:

$$\gamma_z = \mathrm{e}^{cx} = \beta^{-1}, \quad \gamma_y = \mathrm{e}^{-cx} = \beta, \quad \gamma_x = 1,$$

where x is the effective length from the beginning of the distortion to any location in the distortion and c is a tunnel constant. The wind tunnel is described further by Keffer *et al.* (1978).

The nominal width of the flat plate, W, was 6.0 mm (so that the aspect ratio was 36 upstream of the distorting duct) and was located approximately $120W$ upstream of the distortion section. A wind tunnel speed (U_0) of 7.0 m s^{-1} was used, resulting in a Reynolds number based on W of approximately 3000.

Pattern-recognition (PR) results were obtained by means of a rake of six X-wires, positioned in the horizontal plane or the vertical plane (see figure 1). The wires, which measure streamwise (u) and lateral (v) or streamwise (u) and spanwise (w) velocity signals, were calibrated *in-situ* in a larger recirculating wind tunnel prior to being used in the distortion tunnel. Dantec 56C01 and 55M10 constant-temperature anemometers were used in conjunction with a digital data acquisition system. The anemometer

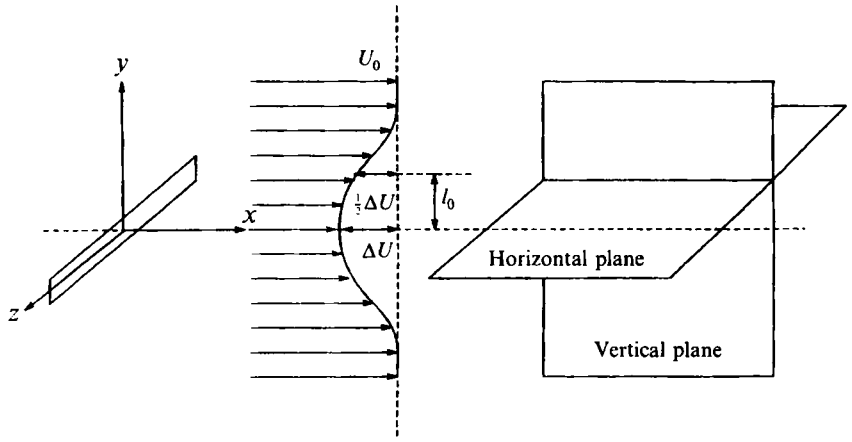

FIGURE 1. Definition sketch.

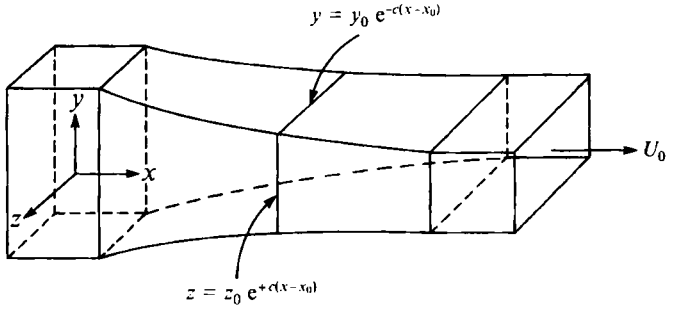

FIGURE 2. Sketch of the distorting duct.

signals were amplified, low-pass filtered at 2000 Hz, sampled at 5000 Hz for approximately 40 s, and stored on an optical disk for later processing on a Sun Sparc station 2. A single X-wire was also used to map out the basic characteristics of the flow. Measurements were taken at nine streamwise locations with the single X-wire, viz. $x/W = 24$, 40, 60, 80, 100, 120, 160 ($\beta^{-1} = 1.2$), 200 ($\beta^{-1} = 1.5$), and 240 ($\beta^{-1} = 1.9$) and at seven locations with the rakes, namely $x/W = 40$, 60, 100, 120, 160 ($\beta^{-1} = 1.2$), 200 ($\beta^{-1} = 1.5$), and 240 ($\beta^{-1} = 1.9$). The X-wire probes were separated by 16 mm, yielding a rake width of 8 cm. At $x/W = 120$ the probe spacing was $0.63l_0$, while at $x/W = 240$, it was $0.80l_0$. At $x/W = 160$, 200, and 240 a probe spacing of 24 mm, corresponding to $1.2l_0$ at $x/W = 240$, was also used in the horizontal plane.

3. Theoretical considerations

Taylor's (1935) rapid distortion theory, applied to the present distorting duct, yields

$$\omega_{z1} = \beta^{-1}\omega_{z0},$$

where ω_z is the vorticity component of the organized flow pattern in the z (spanwise) direction, the subscript 1 indicates any location in the distortion and the subscript 0 indicates a location prior to the distortion; also,

$$\omega_{y1} = \beta\omega_{y0},$$

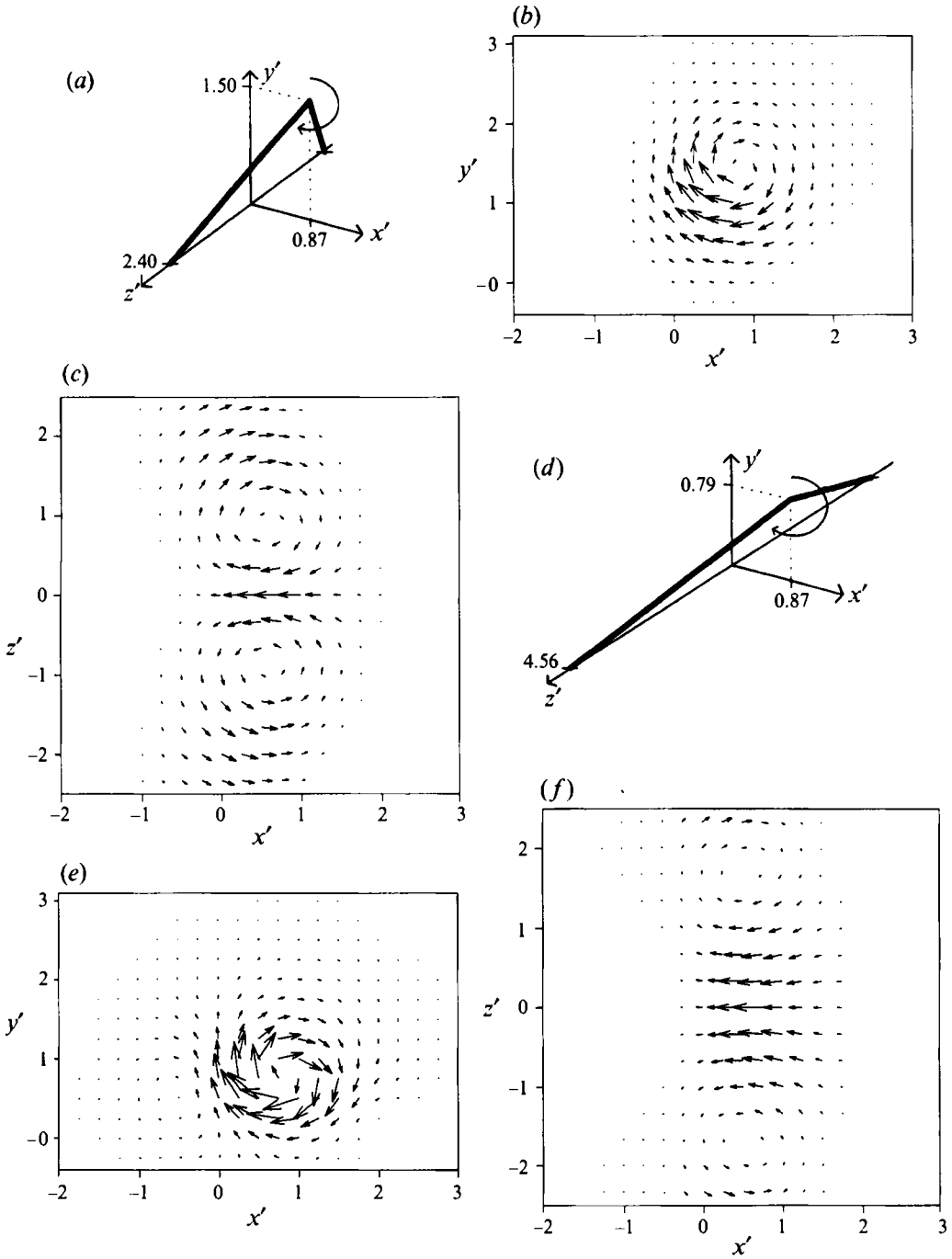

FIGURE 3. Vorticity axes and velocity vectors (either $u\hat{i}+v\hat{j}$ or $u\hat{i}+w\hat{k}$) from the Λ-vortex model: (*a*) vorticity axes, as indicated by the thick line with the arrow indicating the direction of flow in the vertical symmetry plane, of the undistorted vortex model; (*b*) velocity vectors in the vertical symmetry plane; (*c*) velocity vectors in the horizontal plane at $y' = 1.0$; (*d*) vorticity axes when $\beta^{-1} = 1.9$; (*e*) velocity vectors in the vertical symmetry plane, when $\beta^{-1} = 1.9$; and (*f*) velocity vectors in the horizontal plane at $y' = 0.5$ of the distorted vortex, when $\beta^{-1} = 1.9$.

where ω_y is the vorticity component in the y (lateral) direction; and,

$$\omega_{x1} = \omega_{x0},$$

where ω_x is the vorticity component in the x (streamwise) direction. Hence, vorticity in the spanwise direction should be amplified while the vorticity in the lateral direction should be suppressed by the distortion. With a given initial streamline pattern, the corresponding vorticity and velocity fields can be calculated via Poisson's equation,

$$\nabla^2 H_{i1} = -\omega_{i1} \tag{1}$$

where $i = x$, y or z, and H_{i1} are the streamfunctions corresponding to the vorticity components (Taylor 1935).

The kinematic model of the far-wake coherent structures is based on previous experimental results obtained by Ferré *et al.* (1990), Bisset, Antonia & Browne (1990), Giralt & Ferré (1993), and others. Basically, this model is a Λ-vortex inclined in the streamwise direction, 30° from the lateral coordinate. Or, one could think of it simply as two finite line vortices that meet at a point, with an included angle of 116°. Figure 3(*a*) depicts the vorticity axes of the model, with the arrow indicating the direction of the flow in the vertical symmetry plane. The streamfunction along the axis of each line vortex is

$$H_{10} = H_1 \exp\left\{-\frac{1}{2}\frac{r_d^2}{r_1^2}\right\}, \tag{2}$$

where H_1 and r_1 are constants. (This is the same function that is used to generate the template in figure 4*a* for the PR analysis.) Equation (2) is differentiated appropriately to obtain the velocity distribution (see Taylor 1935). This velocity field is then differentiated to obtain the vorticity distribution along the axis of each line vortex. Since both line vortices are inclined with respect to the coordinate axes, a simple coordinate transformation is required to obtain ω_{x0}, ω_{y0}, and ω_{z0}, for each line vortex. The vorticity distributions for both line vortices are then summed and the rapid distortion equations are applied to obtain ω_{x1}, ω_{y1}, and ω_{z1}. Equation (1) is then solved numerically with finite differences and the Gauss–Siedel successive-over-relaxation technique. The resulting velocity field is obtained by numerical differentiation of the streamfunctions (Taylor 1935). The numerical error in the solution of (1) is estimated to be less than 5%.

Figures 3(*b*) and 3(*c*) show the velocity vectors of the vortex model in the vertical (symmetry) plane and the horizontal plane at $y' = 1$, respectively, where $y' = y/l_{120}$, $z' = z/l_{120}$, and $x' = x/l_{120}$ with $l_{120} = l_0$ at $x/W = 120$. The vorticity along the axes of the vortex model (i.e. the axis of each line vortex) is constant. However, because the two line vortices are not parallel, the spanwise vorticity is maximum at the vertex, and this maximum is about twice the maximum lateral vorticity at $y' = 1$.

The uniform distortion has two primary effects on the kinematic model. The first has to do with the vorticity: the distortion amplifies the spanwise vorticity, attenuates the lateral vorticity, and leaves the streamwise vorticity unchanged, as shown above. For example, if $\beta^{-1} = 1.9$, then $\omega_{z1} = 1.9\omega_{z0}$ while $\omega_{y1} = 0.53\omega_{y0}$. The second effect has to do with the location of a vortex centre. The centre of the vortex in the vertical symmetry plane is located at $y' = 1.5$, in the undistorted state, but after the Λ-vortex is distorted, with $\beta^{-1} = 1.9$, the centre moves to $y' = 0.79$, that is, closer to the centre of the wake. As well, the vortex centres in the horizontal plane move apart. Essentially, the Λ-vortex has its legs pulled apart, causing the structure to have a much larger

spanwise extent, as depicted in figure 3(*d*). The resulting vortex now has an included angle of 160° and is inclined 48° in the streamwise direction. The resulting velocity vectors are shown in figures 3(*e*) and 3(*f*), which, again, pertain to the vertical symmetry plane and the horizontal plane at $y' = 0.5$, respectively. These results will be discussed in more detail in §§5 and 6.

At this point, it is appropriate to explain why a single A-vortex was used rather than an array of vortices. We believe that the ensemble-averaged velocity vectors represent the 'average' coherent structure, which the Λ-vortex attempts to model. Accordingly, it is of interest to compare the 'average' coherent structure at the end of the distorting duct with the structure obtained from the rapid distortion analysis of the vortex model. Only if a quasi-periodicity was apparent in the ensemble-averaged results obtained upstream of the distortion would an array of vortices be likely to be necessary to obtain a reasonable comparison with the ensemble-averages prior to and within the distortion.

However, use of an array of vortices, as done by Davies (1976), Bisset *et al.* (1990), and others, would lead to a more accurate modelling of the various wake profiles (e.g. u', v', etc.). Nevertheless, several aspects remain unclear when a three-dimensional model of the complete plane turbulent far wake is considered, namely how and where do the ends of the 'legs' of the Λ-vortices terminate, how do these 'legs' interact with each other, and what is the spanwise distribution of these vortices. Therefore, the objective of the present modelling is to predict and observe the changes in the coherent structures detected with the PR analysis, not to predict the complete far-wake flow.

4. Eduction of coherent structures

The coherence function technique, which is an effective way of indicating the presence of coherent structures with spanwise vorticity, by means of streamwise and lateral velocity signals, for example, has been described by Budny, Kawall & Keffer (1979), and is briefly reviewed here. The Fourier transform of the correlation function of two signals, $\alpha_1(t)$ and $\alpha_2(t)$, is the cross-spectral density function, $E_{12}(n;s)$. Specifically,

$$E_{12}(n;s) = \int_{-\infty}^{+\infty} \rho_{12}(\tau;s)\, e^{-i2\pi n\tau}\, d\tau.$$

In this expression, $s \geqslant 0$ is spatial separation, n is a frequency, τ is a time lag, and $\rho_{12}(\tau;s)$ is the cross-correlation function, i.e.

$$\rho_{12}(\tau;s) = \overline{\alpha_1(t)\,\alpha_2(t+\tau)}/\alpha_1'\,\alpha_2',$$

where α_1' and α_2' are root-mean-square values. The coherence function is given by

$$\Gamma_{12}(n;s) = \frac{C_{12}^2(n;s) + Q_{12}^2(n;s)}{E_{11}(n)\,E_{22}(n)},$$

where $C_{12}(n;s)$ is the real part of $E_{12}(n;s)$ and $Q_{12}(n;s)$ is the imaginary part. $C_{12}(n;s)$ represents the in-phase components of $\rho_{12}(\tau;s)$ while $Q_{12}(n;s)$ represents the 90° out-of-phase components. $E_{11}(n)$ and $E_{22}(n)$ are the auto-spectra of $\alpha_1(t)$ and $\alpha_2(t)$ respectively. It may be remarked that any two signals can be used, but improved detection with this technique would be effected by use of lateral velocity (v) and the spanwise vorticity (ω_z) signals, for example.

The present pattern-recognition technique is a modified version of the technique developed by Ferré & Giralt (1989*a*), which uses a correlation approach to select the individual realizations that make up an ensemble-averaged pattern characterizing a coherent structure. An initial template depicting the structure's velocity footprint is correlated with the velocity signals and the locations within the signals where the correlation exhibits maxima (and exceeds some minimum threshold level) are selected and used for ensemble averaging. An iterative procedure is then used, with the current ensemble-average taken as the template for the next ensemble-average. The threshold used is one standard deviation of the correlation's variation at $x/W = 120$. This corresponds to a correlation of $+0.32$ in the present work. When there is no statistically significant change between successive ensemble-averaged patterns, the procedure is terminated. (Statistical analysis of the relevant data allows the significance levels associated with the patterns to be obtained.)

5. Unstrained far-wake structures

Grant (1958) was the first to give a detailed description of the coherent structures in the far field of a plane turbulent wake. His comprehensive set of correlation measurements implied that the flow contained double roller eddies (with a vorticity axis perpendicular to the spanwise direction and inclined with respect to the lateral direction) and 'spanwise entraining eddies' (with spanwise vorticity). Recently, Bisset *et al.* (1990), Giralt & Ferré (1993), and others have presented data on these eddies obtained with rakes of X-wires, used in conjunction with the VITA and PR techniques, and have concluded that the two types of eddies are in fact a single connected structure, the 'shape' of which is effectively that of a horseshoe.

Figures 4(*b*) and 4(*c*) show the ensemble-averaged velocity fluctuation vectors and the corresponding ensemble-averaged spanwise vorticity fluctuation contours of the spanwise entraining eddies obtained with PR analysis of vertical plane measurements at $x/W = 120$. The initial template that was used is depicted in figure 4(*a*). Four points should be noted here. First, this template does not correspond exactly to the velocity vectors of the vortex model depicted in figure 3(*b*); it corresponds to a single roller, whose vorticity axis is perpendicular to the page. Equation (2) is used to calculate the velocity distribution pertaining to figure 4(*a*). Secondly, the ensemble-averaged vorticity fluctuations are generated from the velocity fluctuation vectors while the contours are obtained by interpolation between the probe locations. Because of the coarse probe spacing, the error in the maximum vorticity could be quite large. However, comparison of the exact vorticity values obtained from the kinematic model and those calculated from the velocity vectors of the model with a spacing similar to that used experimentally indicated that the shapes of the contours were in close agreement, although the peak calculated value could be up to 40% lower than the exact value. Thirdly, with respect to all PR plots, time increases to the left so that the flow is from the left-to-right. On the vector plots, either the $u\hat{i}+v\hat{j}$ or the $u\hat{i}+w\hat{k}$ vectors are plotted. On the contour plots, the contour levels are $\pm 75\%$, $\pm 50\%$, $+25\%$, and $\pm 10\%$ of the peak value for each plot, with the arrows giving the relative magnitude. Arrows pointing to the right are positive, while arrows pointing to the left are negative. The length and time coordinates are non-dimensionalized with the free-stream velocity, U_0, and the mean-velocity half-width lengthscale, l_0. Fourthly, only every other velocity vector is plotted, for clarity.

As can be seen, there is no evidence of quasi-periodicity in the flow at $x/W = 120$, but a circulation pattern can be discerned. Most of the circulatory motion is due to the

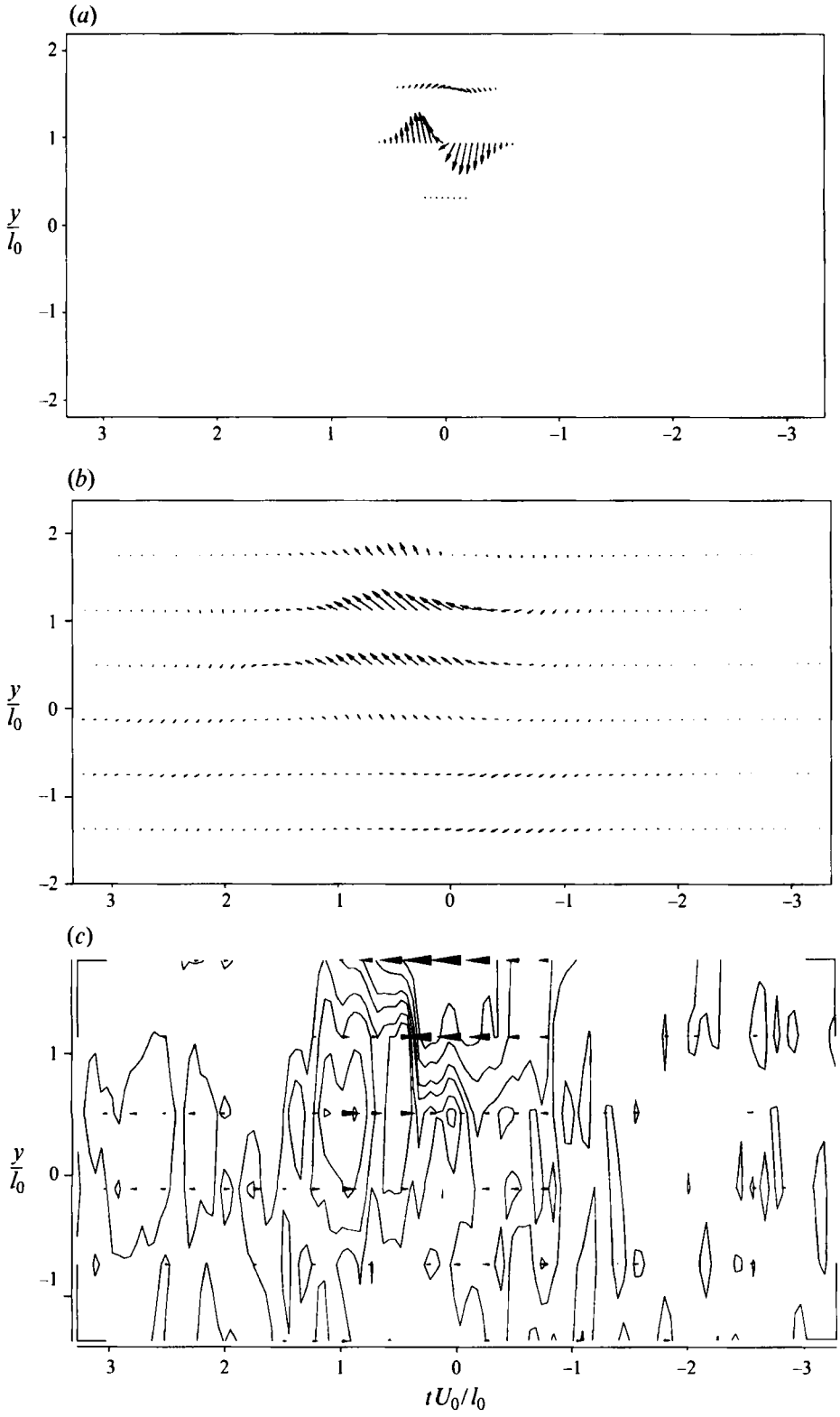

FIGURE 4. For caption see facing page.

back flow associated with the double roller portion of the horseshoe structure. The circulatory pattern in the plot is relatively weak because the velocities are normalized with the free-stream velocity, U_0, after the local mean velocities have been subtracted off. If the velocities were to be normalized with the local streamwise r.m.s. velocity, u', the circulatory pattern would appear stronger. It is noted that Giralt & Ferré's (1993) results are normalized with the local streamwise r.m.s. velocity, u', which has the effect of amplifying the velocities at the outer edge of the wake relative to the rest of the wake. Hence, the circulatory pattern in their figure 2, which corresponds to figure 4(*b*), is stronger. In other words, normalizing figure 4(*b*) with u' would make it appear much the same as Giralt & Ferre's (1993) figure 2. Throughout this paper, the ensemble-averages are presented with the local mean subtracted off and the resulting fluctuations normalized with U_0, in order to facilitate comparison with the RDT results. In addition, the vorticity fluctuation contours are normalized with U_0 and W.

With reference again to figure 4(*c*), it is interesting to note that there is both clockwise and counterclockwise vorticity associated with the ensemble-averaged structure. The clockwise vorticity causes the circulatory motions responsible for the engulfment process (Townsend 1966, 1970; Ferré & Giralt 1989*a*, *b*, and others). The associated circulation is centred at approximately $y = 1.5l_0$. The counterclockwise vorticity has no circulatory motions associated with it in the vertical plane, but it is nearly equal in magnitude to the clockwise vorticity and occurs on the same side of the wake as the latter. This counterclockwise vorticity is also present in the vertical symmetry plane of the vortex model, although the maximum value is only about 20% of the maximum clockwise vorticity.

Figure 5(*b*) shows a slice of the double rollers at $y = l_0$ obtained with PR analysis of horizontal plane measurements at $x/W = 120$. The relevant initial template is depicted in figure 5(*a*). (This template represents two single rollers with lateral vorticity placed in close proximity and is not quite the same as the velocity vectors of the vortex model depicted in figure 3(*c*).) The portion of the ensemble-averaged velocity fluctuation vectors with the negative velocity perturbation (or simply the backflow portion) between the two rolls is responsible for the fine-scale mixing of the engulfed 'non-turbulent' fluid (Ferré & Giralt 1989*a*, *b*). This backflow portion (between the two rolls) is approximately $2l_0$ wide in the z-direction, while the entire structure is approximately $4.5l_0$ wide. These dimensions are essentially the same as those found by Ferré *et al.* (1990) for a cylinder-generated wake at $x/D = 140$ and are half the size of those found by Kopp *et al.* (1995) for a porous-body wake. The centres of the two vortices that make up the double roller are also the centres of the ensemble-averaged vorticity fluctuation contours calculated from the velocity fluctuation vectors. Note that in figures 4(*c*) and 5(*c*), pertaining to the vertical and horizontal planes respectively, the peak vorticities are approximately equal.

(It may be remarked that the ensemble-averaged pattern is not symmetrical about the centreplane. We speculate that this is caused by the rake of probes not being in perfect alignment with the mean flow direction.)

From a comparison of figures 3(*b*) and 4(*b*), pertaining to the vertical plane, and figures 3(*c*) and 5(*b*), pertaining to the horizontal plane, it is evident that the Λ-vortex model and the ensemble-averaged velocity vectors are in reasonable agreement. It

FIGURE 4. The ensemble-averaged velocity fluctuation vectors $u\hat{i}+v\hat{j}$ plotted in the vertical plane: (*a*) the initial template, (*b*) the resulting ensemble-average after four iterations, and (*c*) the ensemble-averaged vorticity fluctuation contours, at $x/W = 120$. The peak streamwise and lateral velocities, relative to U_0, are 0.069 and 0.054, respectively. The peak vorticity ($\omega_z W/U_0$) is -4.4×10^{-5} with contours shown for $\pm 75\%$, $\pm 50\%$, $\pm 25\%$, and $\pm 10\%$ of this value.

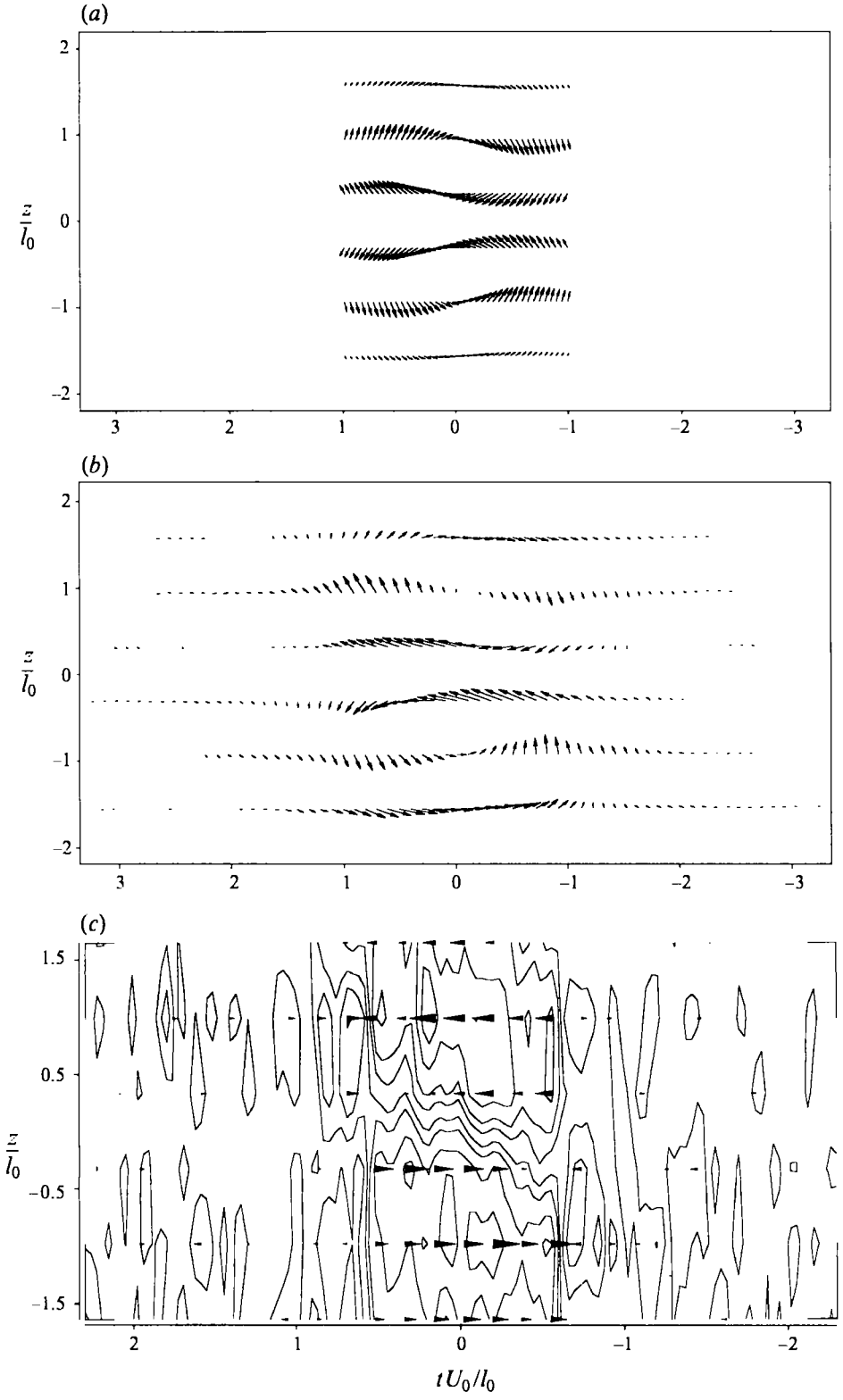

FIGURE 5. For caption see facing page.

should be kept in mind, however, that the vertical and horizontal planes should be examined simultaneously in order to determine with certainty that the two structures are connected.

6. Evolution of the structures in the distorting duct

6.1. *Experimental results*

6.1.1. *Mean velocity lengthscales and r.m.s. profiles*

Figure 6(*a*) depicts the evolution of the mean velocity half-width lengthscale, l_0, as the flow develops from the intermediate wake to the far wake, and then through the distortion. It can be seen that l_0 increases rapidly in the near and intermediate wake and less rapidly as the velocity profile becomes self-similar and the Kármán vortex street disappears; it then decreases through the distorting duct as the imposed strain compresses the wake in the lateral direction and stretches it in the spanwise direction. This particular lengthscale varies in a manner consistent with the predicted self-preserving solution for the present uniform distortion and the RDT predictions. (The l_0 pertaining to the RDT predictions needs some explanation because there is no mean defect present with the undistorted kinematic model. We find that $u_0/U_d \sim 10$, where u_0 denotes the centreline value of the streamwise r.m.s. velocity, u', and U_d the maximum velocity defect, whereas experimentally, at $x/W = 120$, $u_0/U_d \sim 1/3$. Therefore, the predicted l_0 is assumed to be proportional to the lateral extent of the Λ-vortex.) Figure 6(*b*) depicts the evolution of the maximum velocity defect, U_d. The amplification of spanwise vorticity causes this defect to decrease less rapidly in the distorted wake than in the undistorted wake and at about the same rate as that predicted by the self-preserving solution for the distorted wake.

Figure 6(*c*) depicts the evolution of the lateral r.m.s. velocity intensity scale, v_0, defined as the centreline value of the lateral r.m.s. velocity, v'. This figure clearly shows that the distorted wake is not self-preserving, because v_0 remains nearly constant rather than decaying exponentially as predicted. RDT, on the other hand, predicts that v_0 should increase, owing to the predicted increase of the spanwise vorticity as the flow evolves. This figure also indicates that RDT, when applied to a kinematic vortex model, is inconsistent with self-preserving theory, even though both theories predict reasonably well the evolution of the mean-velocity lengthscale (l_0) of the distorted wake.

Figures 6(*d*) and 6(*e*) illustrate how the ratios of lateral r.m.s. intensity scale, v_0, and spanwise r.m.s. intensity scale, w_0, to the streamwise r.m.s. intensity scale, u_0, change during the distortion. As can be seen, v_0/u_0 increases due to the imposed strain, whereas the self-preserving theory predicts that it should remain constant. On the other hand, RDT does a good job predicting the observed variation, even though the actual magnitudes of u_0 and v_0 are overestimated. As well, w_0/u_0 decreases slightly through the distortion, with RDT substantially underestimating this ratio and self-preserving theory overestimating it.

Figure 6(*f*) displays the streamwise r.m.s. velocity, u', profiles obtained experimentally and with RDT applied to the Λ-vortex. (The RDT r.m.s. profiles are

FIGURE 5. The ensemble-averaged velocity fluctuation vectors $u\hat{i} + w\hat{k}$ plotted in the horizontal plane: (*a*) the initial template, (*b*) the resulting ensemble-average after four iterations, and (*c*) the ensemble-averaged vorticity fluctuation contours at $x/W = 120$ and $y/l_0 = 1.0$. The peak streamwise and spanwise velocities, relative to U_0, are 0.047 and 0.031, respectively. The peak vorticity ($\omega_y W/U_0$) is -4.0×10^{-5} with contours shown for $\pm 75\%$, $\pm 50\%$, $\pm 25\%$, and $\pm 10\%$ of this value.

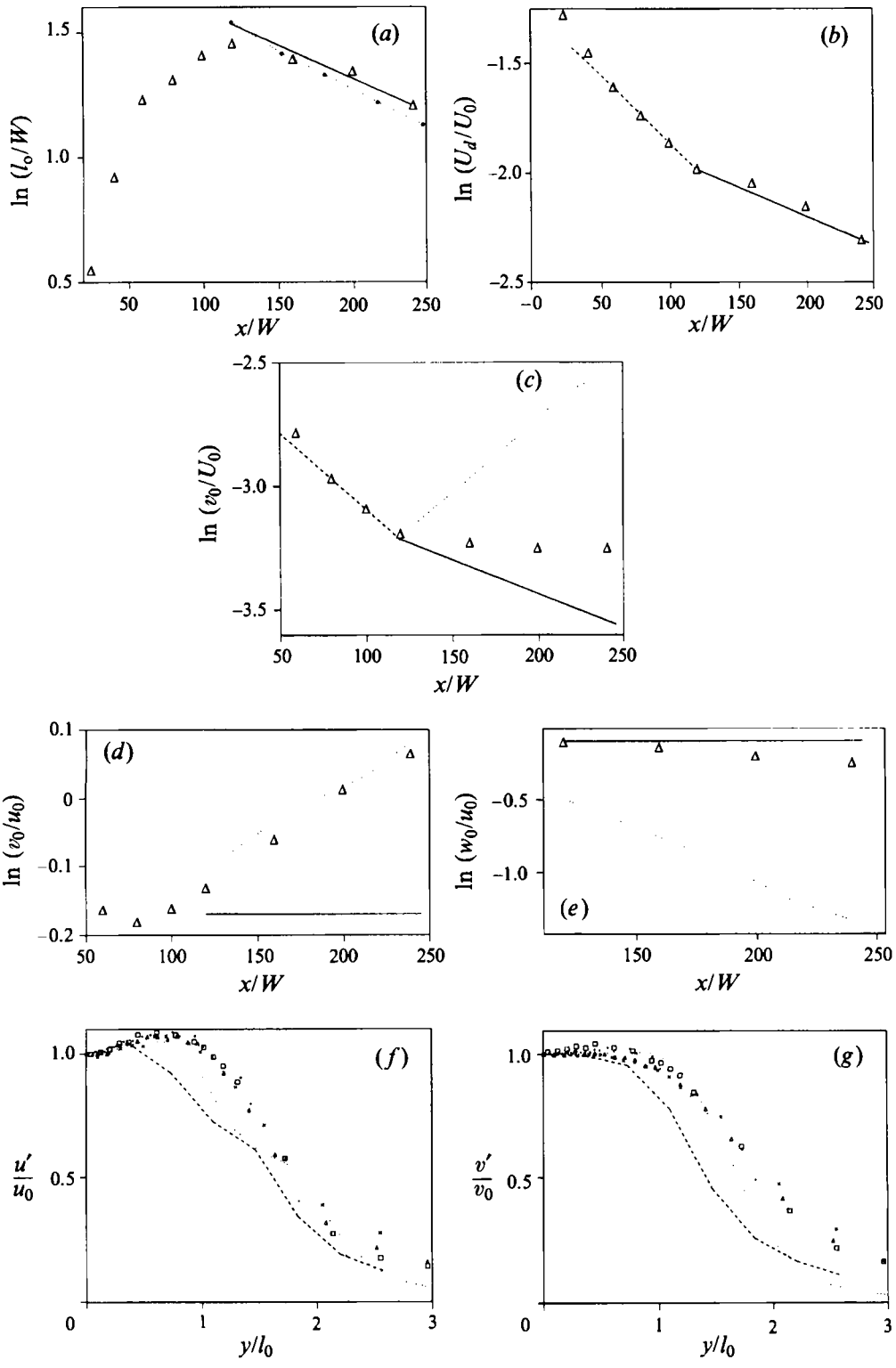

FIGURE 6. For caption see facing page.

calculated by averaging over the entire x, z (horizontal) plane for each y-location used in the computational grid.) This figure shows that the vortex model provides a reasonable estimate of the self-similar profile, but it underestimates this profile when RDT is applied, although it still predicts a peak away from the centreline. Note that in the case of the distorted wake, the predicted profile depends on β^{-1}, becoming narrower as β^{-1} increases, even though l_0 is slightly underestimated. Figure 6(g) displays the lateral r.m.s. velocity, v', profile. This figure shows that v' is approximately self-similar experimentally, though with more scatter than in the case of u'. Again, the undistorted Λ-vortex does a reasonable job estimating the experimental profile. RDT, however, predicts that the peak value moves towards the centreline and, again, underestimates the experimental profile. (The w' profiles show similar behaviour.)

If an array of Λ-vortices were used (say, in a manner similar to the distribution described by Bisset *et al.* 1990), the predicted distorted wake profiles would never be exactly self-similar because the uniform distortion field has the effect of moving vortex centres in the vertical plane towards the centreline, causing the normalized profiles to become 'thinner'. However, this effect would be less pronounced with an array than with a single vortex. It is, therefore, interesting, and surprising, that a single Λ-vortex can predict reasonably well the measured r.m.s. profiles, although this single vortex is not proposed as a model of the entire far wake flow.

6.1.2. *Spectral analysis and coherence function measurements*

Prior to the distortion section, at $x/W = 120$ and $y/l_0 = 1.0$, the v-autospectrum, presented in figure 7(a), exhibits little evidence of any frequency-centred activity. However, the coherence function, Γ_{uv}, presented in figure 7(b), displays frequency-centred activity in the 20–50 Hz range with a peak of 0.4 at 40 Hz. By $x/W = 240$ ($\beta^{-1} = 1.9$) and $y/l_0 = 1.0$, a large broadband peak has appeared in the v-autospectrum in the range 40–80 Hz, as can be seen in figure 7(c). This peak is centred at approximately 60 Hz, which is one-third of the characteristic Strouhal shedding frequency (180 Hz). Γ_{uv} shows a peak in about the same frequency range as that occurring at $x/W = 120$, but the peak is stronger, being approximately 0.6 at 50 Hz, as can be seen in figure 7(d).

6.1.3. *Pattern-recognition analysis (vertical plane)*

Ensemble-average results from the vertical-plane PR analysis are presented in figure 8. The relevant initial template is shown in figure 4(a). It is apparent that the central structure, a spanwise vortex, with clockwise rotation (from the top of the wake) has been joined by another structure, also a spanwise vortex, with counterclockwise rotation (from the other side of the wake) on its upstream side. This is clear evidence that quasi-periodicity appears in the flow. There is still slight evidence of the presence of double rollers between the two spanwise vortices, but it is likely that their vorticity would be primarily in the streamwise direction. The most striking aspect of figure 8(a), however, is the fact that the spanwise vortices now extend across almost the entire wake (about $4l_0$). We note that this is similar to the situation in the near region of a plane porous-body wake (Huang *et al.* 1993). The velocity vectors in this figure, and the corresponding vorticity distribution, have an unusual appearance because the local mean velocity has been subtracted off. (They would have a more conventional

FIGURE 6. (a) $\ln(l_0/W)$ *vs.* x/W, (b) $\ln(U_d/U_0)$ *vs.* x/W, (c) $\ln(v_0/U_0)$ *vs.* x/W, (d) $\ln(v_0/u_0)$ *vs.* x/W, (e) $\ln(w_0/u_0)$ *vs.* x/W: △, from experiments; – – –, curve-fit to pre-distortion data; ——, self-preserving theory; ....., rapid distortion theory. (f) Streamwise r.m.s. velocity, u'/u_0 *vs* y/l_0, and (g) lateral r.m.s. velocity, v'/v_0 *vs.* y/l_0: △, $x/W = 240$; ×, $x/W = 200$; □, $x/W = 160$; ·, $x/W = 120$; ·····, Λ-vortex, undistorted; – – –, Λ-vortex, distorted with $\beta^{-1} = 1.9$.

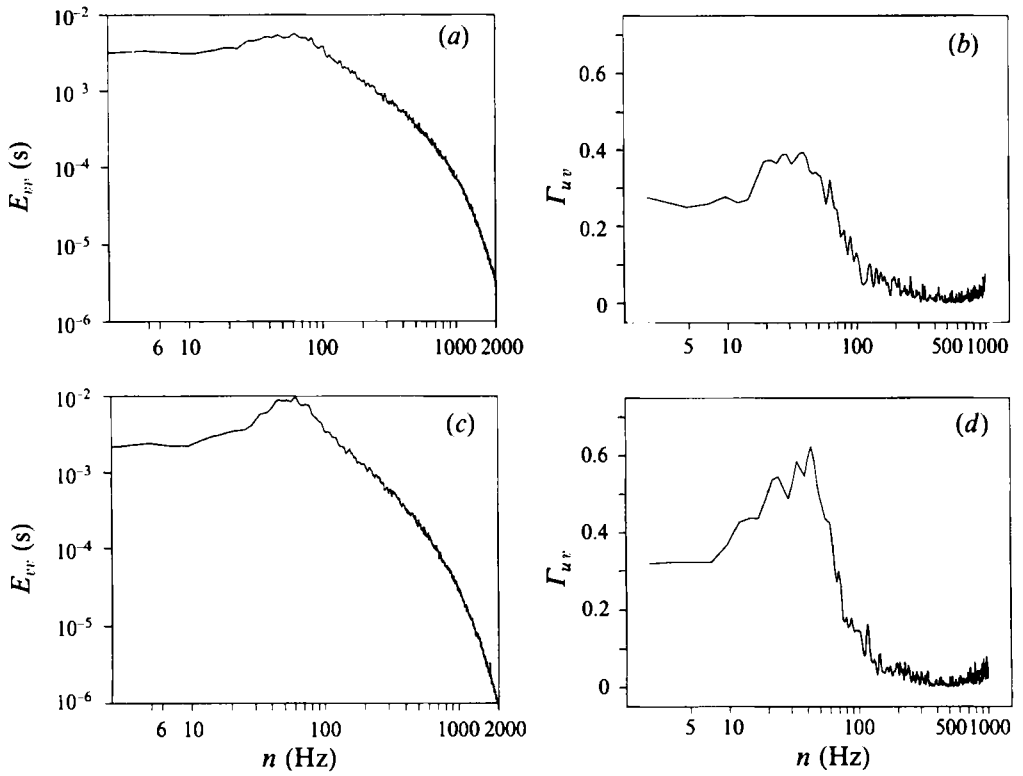

FIGURE 7. Spectral analysis results: (*a*) E_{vv} and (*b*) Γ_{uv}, for $x/W = 120$ and $y/l_0 = 1.0$; (*c*) E_{vv} and (*d*) Γ_{uv}, for $x/W = 240$ and $y/l_0 = 1.0$.

appearance with a convection velocity present.) Clearly, these spanwise structures dominate the flow.

From a comparison of figures 4(*b*) and 8(*a*), it appears that the temporal scale of the spanwise vortices has increased, while this apparent increase in scale is not exhibited when figures 3(*b*) and 3(*e*), pertaining to the vortex model, are compared. However, comparisons of the ensemble-averaged vorticity fluctuation contours in figures 4(*c*) and 8(*b*) leads to the conclusion that the distorted structures are of only a slightly larger temporal scale. Why then do the velocity fluctuation vectors appear to span a much larger temporal (or streamwise) extent than that predicted by RDT? There are several possible reasons for this. First, there must be some diffusion of vorticity, which leads to increased lateral and streamwise scales of the velocity vectors. Secondly, quasi-periodicity of the coherent structures leads to increased lateral velocities between any two adjacent spanwise vortices, which, in conjunction with the enhanced spanwise vorticity, makes the scale of the ensemble-averaged structures and the vortex model appear to be different, at first glance.

Table 1 indicates that the ratio of the peak ensemble-averaged lateral and streamwise velocities, obtained from the PR analysis, increases through the distortion and becomes greater than unity, consistent with the r.m.s. intensity scales and RDT predictions, although at a much greater rate. As well, the peak spanwise coherent vorticity remains roughly constant through the distortion as does the lateral intensity scale, v_0. This is indirect evidence that the coherent structures are responsible for the failure of the distorted wake to undergo a self-preserving development (as will be discussed further in §6.2).

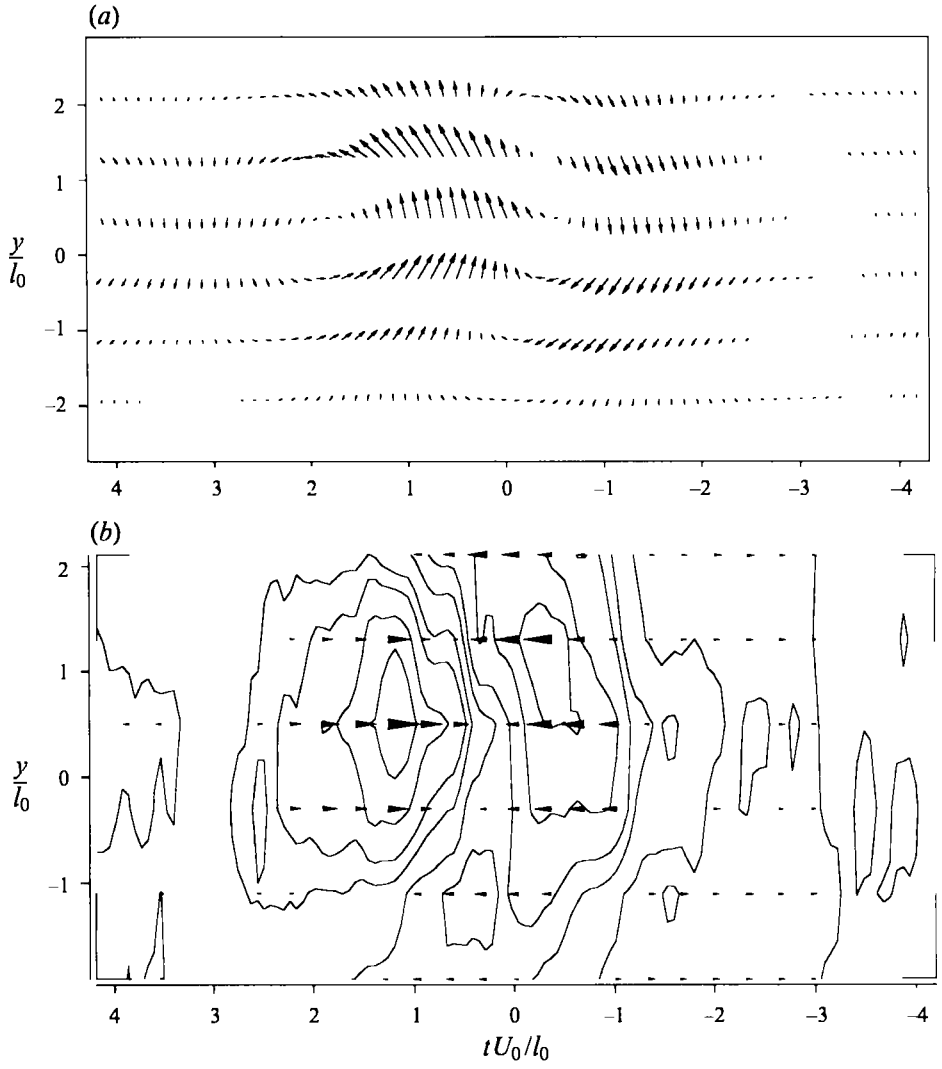

FIGURE 8. The ensemble-averaged velocity fluctuation vectors $u\hat{i}+v\hat{j}$ plotted in the vertical plane, with (*b*) the ensemble-averaged vorticity fluctuation contours, at $x/W = 240$. The peak streamwise and lateral velocities, relative to U_0, are 0.032 and 0.044, respectively. The peak vorticity ($\omega_z W/U_0$) is -4.3×10^{-5} with contours shown for $\pm 75\%$, $\pm 50\%$, and $\pm 10\%$ of this value.

β^{-1}	x/W	$v_{c,max}/u_{c,max}$ vertical plane	$w_{c,max}/u_{c,max}$ horizontal plane	$\omega_{z,max}/\omega_{y,max}$ Experiment	Theory
1.0	120	0.73	0.63	1.1	1.1
1.2	160	0.71	0.43	1.6	1.6
1.5	200	0.89	0.40	1.7	2.5
1.9	240	1.39	0.41	2.1	4.0

TABLE 1. Peak coherent vorticity ratios and peak coherent velocity ratios in the distorting duct from the PR analysis

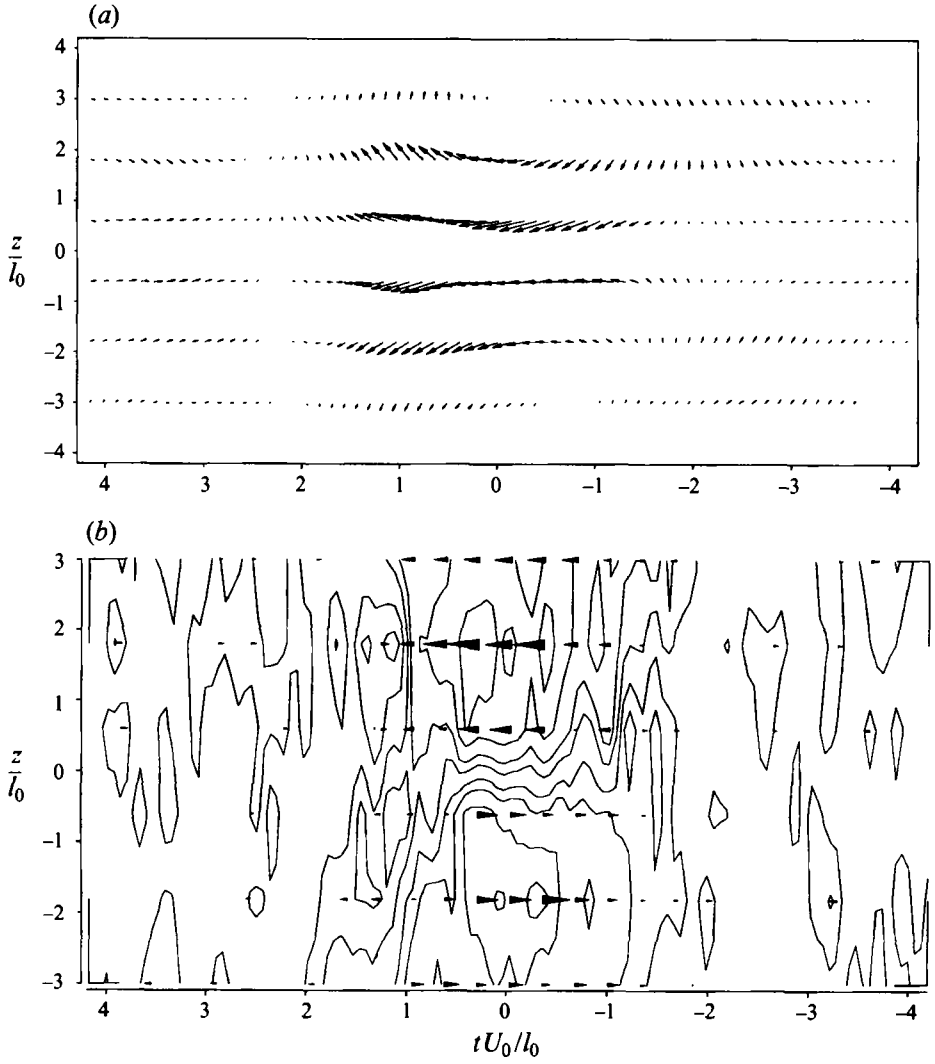

FIGURE 9. The ensemble-averaged velocity fluctuation vectors $u\hat{i}+w\hat{k}$ plotted in the horizontal plane, with (*b*) the ensemble-averaged vorticity fluctuation contours, at $x/W = 240$ and $y/l_0 = 1.0$. The peak streamwise and spanwise velocities, relative to U_0, are 0.044 and 0.018, respectively. The peak vorticity ($\omega_y W/U_0$) is -2.0×10^{-5} with contours shown for $\pm75\%$, $\pm50\%$, $\pm25\%$, and $\pm10\%$ of this value.

6.1.4. *Pattern-recognition analysis (horizontal plane)*

Ensemble-average results from the horizontal-plane PR analysis are presented in figure 9. The relevant initial template is shown in figure 5(*a*). By the end of the distortion ($x/W = 240$, $\beta^{-1} = 1.9$), the distance between the two vortex centres is slightly larger than the 12 cm wide rake ($6l_0$ wide). This width is about 20% greater than that predicted from RDT. From this figure 9, as well as figure 3(*f*), it appears, again, that the spanwise portion of the structures dominate the flow. Also, the centres of the ensemble-averaged vorticity fluctuation contours for each of the two rolls move away from the vortex centres towards the middle of the structure, indicating that the top portions of the horseshoe structures dominate the flow. Hence, the double rollers become strongly attenuated and the coherent structures quasi-two-dimensional. It

	Vertical plane		Horizontal plane	
x/W	1st iteration	Converged	1st iteration	Converged
120	1787	935	1126	998
160	1525	809	1009	839
200	1613	1191	951	788
240	1895	1522	994	816

TABLE 2. Number of realizations used to make up the ensemble-averaged velocity vectors, obtained from the PR analysis

should also be noted that the temporal scale of these structures has not changed, as is clearly seen by examining figures 5 and 9.

From examination of figures 5(*b*) and 3(*c*), and a comparison with figures 9(*a*) and 3(*f*), it seems likely that the double rollers and spanwise vortices are connected in a manner similar to that assumed by the kinematic model. If the double rollers occur by themselves, the backflow portion between the two vortex centres would be weaker and the ratio of maximum w-velocity to maximum u-velocity from the ensemble-average would be constant or increase, unless they have some spanwise vorticity. Table 1 indicates that the ratio of the peak coherent spanwise velocity to the peak coherent streamwise velocity from the ensemble average decreases about 35% (the peak lateral vorticity decreases by 50%) as the structures move through the strain field. This indicates that the double rollers have at least some spanwise vorticity, and it is likely that they are connected to the spanwise vortices, as assumed by the Λ-vortex model. The ratio of peak spanwise vorticity to peak lateral vorticity more than doubles as the flow evolves, as shown in table 1, again indicating the dominance of the spanwise vortices. This increase of the vorticity ratio is, however, somewhat less than that predicted theoretically (using the experimentally obtained peak coherent vorticities as the initial condition).

6.1.5. *Intervals between successive pattern recognition detections*

Table 2 presents the number of realizations that the PR technique selected to educe the ensemble-averages. At $x/W = 120$, the number of realizations selected for the horizontal-plane and vertical-plane analyses are nearly equal. As the flow develops, it is clear that the number of realizations selected in the vertical-plane analysis increases, while, for the horizontal-plane analysis, there is a decrease in the number selected: by $x/W = 240$, there are nearly twice as many selected in the vertical-plane analysis as in the horizontal-plane analysis.

It should be noted that the choice of threshold affects the number of realizations selected. However, using a different threshold does not affect the ratio of the number of realizations selected at $x/W = 240$ to the number selected at $x/W = 120$ as long as the same threshold is used at both stations. In addition, changing the threshold does not significantly change the 'appearance' of the ensemble-averaged patterns or the evolution of the ratios of the peak values, but it does change the magnitude of the peak values of velocity and vorticity significantly.

If the time interval between successive detections is inverted, the 'frequency content' of the detections can be obtained. These histograms are somewhat dependent, but not to a large extent, on the choice of threshold used. Hence, they are most useful for comparison purposes, when a constant threshold is used, as is the case here. Figure 10(*a*) shows that at $x/W = 120$, prior to the strain field, the histograms of the inverse

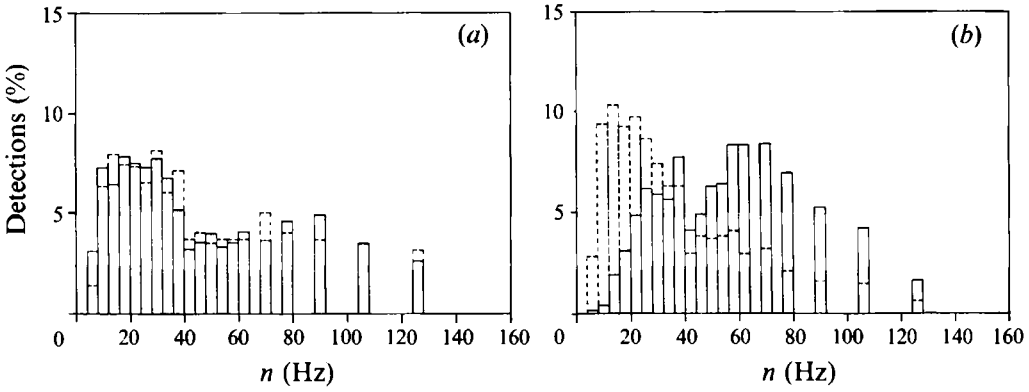

FIGURE 10. Histograms of the detection frequencies from the PR analysis: —, vertical plane and – – –, horizontal plane, at (*a*) $x/W = 120$ and (*b*) $x/W = 240$.

of the interval between successive detections (hereafter called the histograms of detection frequencies) are nearly the same for both the vertical and horizontal planes, with the peak detection frequencies in the range from 16 to 36 Hz, consistent with the notion that the spanwise vortices and the double rollers are parts of the same structure. By $x/W = 240$, the histograms of the detection frequencies have separated, with the central frequencies shifted to approximately 60 Hz for the vertical plane, and about 14 Hz for the horizontal plane. The vertical plane detection frequencies are, thus, consistent with both the v-autospectrum and coherence function measurements.

6.2. *Discussion of results*

6.2.1. *Spatial arrangement of the distorted structures*

When the wake is subjected to the distortion field, it is seen to be dominated by two alternating rows of quasi-two-dimensional structures. We believe that this regular spatial pattern is observed because the coherent structures become increasingly two-dimensional within the distortion. Upstream of the latter, the structures are randomly located in the spanwise direction (although they have a mean lateral location in the vertical plane). Hence, many structures pass through the wind tunnel undetected. As the structures become elongated in the spanwise direction, as a result of being distorted, fewer of them can pass undetected, because they extend across a larger span of the flow. This could be the reason that the distorted wake acquires a quasi-periodicity.

We believe that there are about the same number of coherent structures in the undistorted and distorted regions of the wake, they are just easier to detect in the distortion because of the amplified spanwise vorticity and the fact that they become quasi-two-dimensional. The implication here is that the vortices that were originally in an opposing mode (Bisset *et al.* 1990) within the undistorted far wake move into alignment with the alternating mode (or are obliterated), so that the stable, alternating configuration similar to that which von Kármán predicted (see Lamb 1932) results. It seems likely that the coherent structures that existed upstream of the distorting duct survive through the duct because of the vortex stretching imposed by the distortion. This vortex stretching enhances spanwise vorticity, not allowing the possible growth–decay cycle suggested by Townsend (1966) to occur.

The quasi-periodicity in the distorted wake is consistent with the spectral frequency, which is approximately 60 Hz (figure 7*c*), and with the dominant peak in the histogram

of the intervals between successive detections (figure 10*b*). Figure 8(*a*) is consistent with this frequency, in that the time between the two structures from opposite sides of the wake corresponds to a nominal frequency of about 130 Hz, which is roughly twice the frequency of the spectral peak, as expected.

Further examination of figures 8 and 9 also raises the question as to why the leftmost vortex in figure 8(*a*), with counterclockwise vorticity, appears to be situated very near to the centreline of the wake. This implies that the angle of inclination in the streamwise direction is 90°, or that the legs of the Λ-vortex protrude into the 'wrong' side ($y > 0$) of the wake. A possible explanation for this is based on that for why there is a quasi-periodicity in the distorted wake. Since it is probable that the vortices are randomly distributed in the spanwise direction, it seems unlikely that each vortex that passes the rake of probes is in perfect alignment in the centreplane. (That is, we are not educing the vertical symmetry plane of the Λ-vortices with the PR technique. This could also be the cause of some of the observed variation in the lateral location of the coherent structures.) Because of this spanwise misalignment of adjacent vortices observed in the vertical plane, the legs of the Λ-vortices are included in the ensemble-average, causing the vortex centre to be much closer to the centreline than if only the symmetry planes are educed. Hence, when we educe an ensemble-averaged coherent structure with clockwise vorticity, the adjacent structures, with counterclockwise vorticity, could be centred more closely to the centreline. However, it is still unclear where the legs of these Λ-vortices terminate (or how they interact with other vortices in the core of the wake).

6.2.2. *Entrainment*

The entrainment mechanism in undistorted plane turbulent wakes has been discussed extensively in the literature (e.g. Townsend 1966, 1970; Ferré & Giralt 1989*a*, *b*, and others). In the far wake, the tops of the horseshoe eddies are primarily responsible for engulfing non-turbulent fluid and the legs (or double rollers) primarily responsible for the fine-scale mixing. Figures 11(*a*) and 11(*b*) portray the ensemble-averaged fine-scale turbulence indicator function (FSTIF) in vertical and horizontal planes, respectively, at $x/W = 240$. The FSTIF is the sum of the envelopes of the second derivatives of the u- and v-velocity signals in the vertical plane, and of the u- and w-velocity signals in the horizontal plane, as described by Ferré *et al.* (1990). The FSTIF gives an indication of the instantaneous fine-scale turbulence activity. In figures 11(*a*) and 11(*b*), the FSTIF has been normalized by 'global' variables, rather than local ones. In particular, the mean and r.m.s. values of the FSTIF from the six X-wires at $x/W = 240$ have been used for the normalization. (These values are 1.45×10^6 m s^{-3} and 1.3×10^6 m s^{-3}, respectively.) Hence, negative values would be expected at the edge of the wake and positive values in the core of the wake.

In the vertical plane, figure 11(*a*) indicates that the non-turbulent fluid is engulfed on the downstream side of the spanwise structure and becomes fully turbulent on the upstream side. In the horizontal plane, at $y = l_0$, it is evident from figure 11(*b*) that the mixing is still three-dimensional, on the average, with less turbulent fluid at the outer edges of the double rollers and becoming most intense between the two rolls. Even though the double rollers become large and diffuse, they still play a role in the mixing.

Figure 11(*a*) actually resembles the near region of a porous-body wake (see Huang *et al.* 1993, figure 2), although the present distorted wake is not nearly as organized. There is a fundamental difference, however, in that the porous-body near wake has 'ribs' which enhance the mixing rate, whereas the distorted wake has diffuse double rollers. In addition, the horizontal plane of the porous near wake, the ensemble-

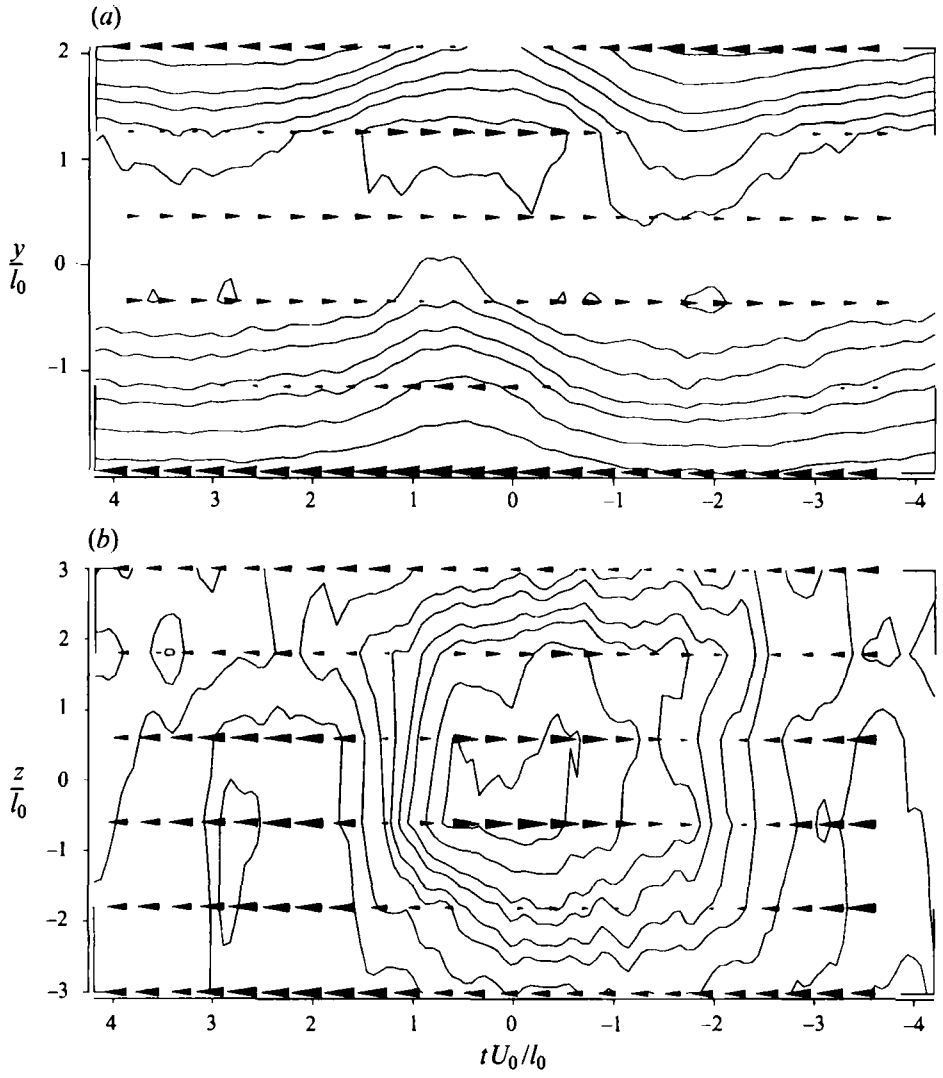

FIGURE 11. The ensemble-averaged fine-scale turbulence indicator function (FSTIF) contours, at $x/W = 240$: (*a*) vertical plane and (*b*) horizontal plane. The peak value of the normalized FSTIF is -0.871, with contours shown for $\pm 75\%$, $\pm 50\%$, $\pm 25\%$, and $\pm 10\%$ of this value.

averaged FSTIF contours are strongly two-dimensional, whereas in the present distorted wake the ensemble-averaged FSTIF contours are three-dimensional (figure 11*b*).

Figure 12 shows a plot of the 'mean volume' of the wake, which is proportional to $l_v \beta^{-1}$ in the distorted wake and l_v in the undistorted wake, where l_v is the local lengthscale for the lateral r.m.s. velocity and is the y-location where v' attains half of its centreline value. The rate of entrainment is proportional to the time rate of change of the mean volume of the flow, so the slope of $l_v \beta^{-1}/W$ versus x/W is proportional to the rate of entrainment in the distorted wake. Since, as figure 12 shows, the curve has a positive slope in the distortion region, the distorted wake grows, or entrains fluid, at an increasing rate, whereas the undistorted wake entrains at a decreasing rate. It appears as if the vortex stretching of the coherent structures causes the entrainment

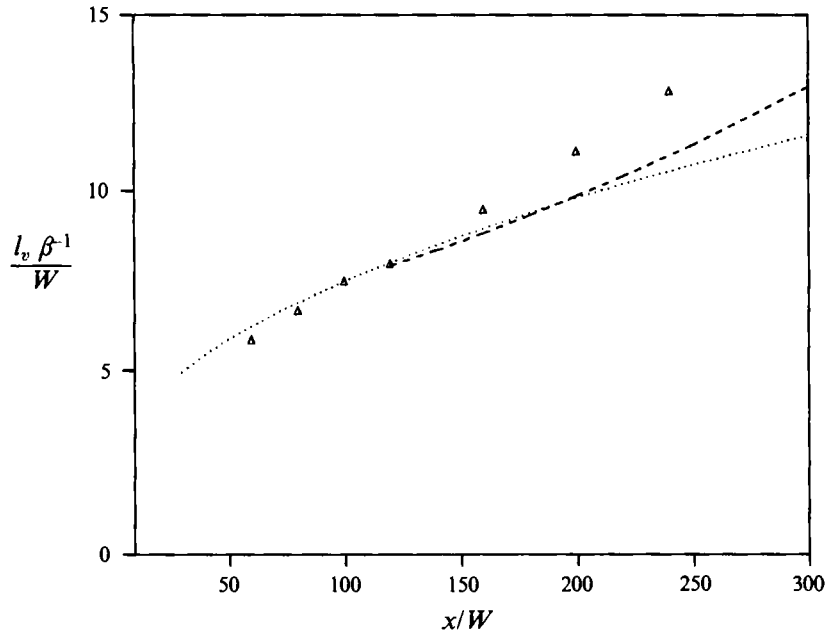

FIGURE 12. The mean volume of the wake, $l_v\beta^{-1}/W$: △, from experiments; ---, self-preserving theory for a uniformly distorted wake; · · · · · ·, self-preserving theory for an undistorted plane wake.

rate to increase. Since these eddies are not allowed to decay, because of the imposed external strain, they continue to entrain fluid, and the growth–decay cycle suggested by Townsend (1966) cannot occur.

6.2.3. *Self-preservation*

Kawall & Keffer (1982) suggested that the uniformly distorted turbulent wake does not become self-preserving because the intermittent turbulent bulges of the flow, which are manifestations of the coherent structures, grow in the distorted wake, rather than become smaller, as predicted from the distorted self-preserving theory. Figure 6(*c*) shows that the lateral r.m.s. velocity intensity scale also is not consistent with the self-preserving theory. It seems likely that this is due to the fundamental changes in the coherent structures, as can be inferred from an examination of figure 8(*a*), which shows that the lateral velocity appears to dominate the coherent motion. Of course, at all scales, v' should be amplified with respect to u' (Townsend 1954), so the issue is whether or not the large scales of v' are amplified disproportionately with respect to the smaller scales. To investigate this point, a 'typical isotropic eddy' is kinematically modelled with the following velocity distribution:

$$u_0 = A_0 \cos(ax_0) \sin(by_0) \sin(cz_0),$$
$$v_0 = B_0 \sin(ax_0) \cos(by_0) \sin(cz_0),$$
$$w_0 = C_0 \sin(ax_0) \sin(by_0) \cos(cz_0).$$

Taylor (1935) used RDT to solve the effect of a distortion on this velocity distribution, yielding

$$u_1 = A_1 \cos(ax) \sin(b\beta^{-1}y) \sin(c\beta z),$$
$$v_1 = B_1 \sin(ax) \cos(b\beta^{-1}y) \sin(c\beta z),$$
$$w_1 = C_1 \sin(ax) \sin(b\beta^{-1}y) \cos(c\beta z),$$

where A_1, B_1, and C_1 depend on A_0, B_0, C_0, and β^{-1}.

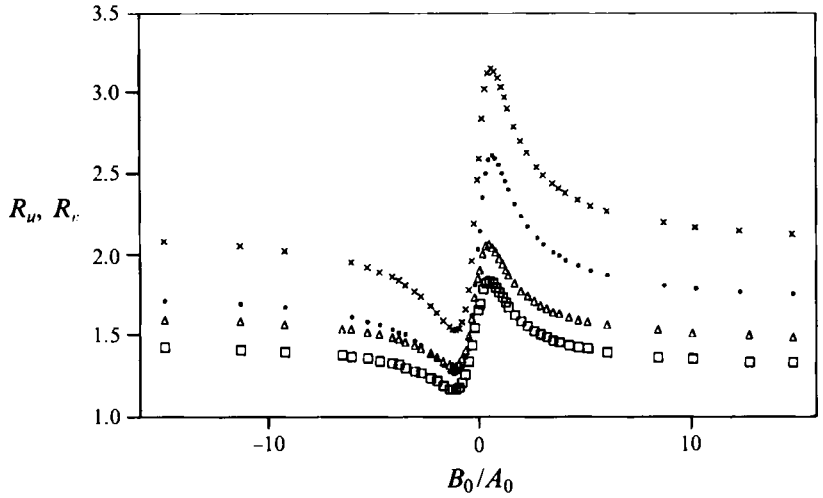

FIGURE 13. Amplification ratios, R_u and R_v, pertaining to the large-scale coherent structures and the small-scale 'isotropic' eddies: □, R_u for $\beta^{-1} = 1.5$; ·, R_v for $\beta^{-1} = 1.5$; ·, R_u for $\beta^{-1} = 1.9$; ×, R_v for $\beta^{-1} = 1.9$.

It seems reasonable to suppose that $a = b = c$ for an isotropic eddy (Taylor 1935). Hence, $A_0 + B_0 + C_0 = 0$ to satisfy continuity. Undistorted isotropic eddies (with a random orientation) would be characterized best by their turbulence energy, which is proportion to $(A_0^2 + B_0^2 + C_0^2)^{1/2}$. The distorted eddies would then be characterized by $(A_1^2 + B_1^2 + C_1^2)^{1/2}$. Accordingly, the amplification ratios are defined as

$$R_v = \frac{v_{0,1}[1 + (B_0/A_0)^2 + (C_0/A_0)^2]^{1/2}}{v_{0,0}[(A_1/A_0)^2 + (B_1/A_0)^2 + (C_1/A_0)^2]^{1/2}},$$

and R_u is similarly defined, but with $u_{0,1}$ and $u_{0,0}$, where $v_{0,1}$ (or $u_{0,1}$) is v_0 (or u_0) in the distortion and $v_{0,0}$ (or $u_{0,0}$) is v_0 (or u_0) prior to the distortion, as predicted from the RDT analysis applied to the Λ-vortex. These ratios represent the amplification ($R_v, R_u > 1$) or attenuation ($R_v, R_u < 1$) of the large-scale coherent structures relative to the smaller scales.

Figure 13 shows that R_u and R_v are greater than unity for all values of B_0/A_0 and C_0/A_0. This strongly suggests that, indeed, the large scales of u' and v' are amplified disproportionately with respect to the smaller scales and that the changes to the coherent structures serve to prevent self-preservation from occurring. Thus, the coherent structures control the development of the distorted wake.

7. Conclusions

A uniform distortion imposed on a plane turbulent wake causes the coherent structures in the undistorted far-wake, horseshoe-like vortices, to become stretched in the spanwise direction and attenuated in the lateral direction. The spanwise vorticity of the coherent structures is disproportionately amplified causing nearly two-dimensional vortices with a quasi-periodicity to reappear in the wake. This fundamental change in the coherent structures prevents the distorted wake from attaining a self-preserving state. Rapid distortion theory, applied to a kinematic model of the undistorted far-wake horseshoe vortices, predicts the observed effects of the distortion

upon the coherent structures reasonably well: specifically, the changes in the ensemble-averaged velocity patterns and the disproportionate amplification of the large-scale coherent structures relative to the smaller 'isotropic' eddies. It can thus be concluded that the coherent structures control the development of the uniformly distorted plane turbulent wake. As well, the vortex stretching imposed on the flow by the external strain does not allow the 'entrainment eddies' to decay, causing the entrainment rate to increase as the distorted wake develops.

This research was supported by NSERC through research grant A-2746. Thanks are due to J. A. Ferré and F. Giralt for the use of their pattern-recognition software. This research is a portion of G. A. Kopp's PhD thesis at the University of Toronto.

REFERENCES

BATCHELOR, G. K. & PROUDMAN, I. 1954 The effect of rapid distortion of a fluid in turbulent motion. *Q. J. Mech. Appl. Maths* **7**, 83–103.

BISSET, D. K., ANTONIA, R. A. & BROWNE, L. W. B. 1990 Spatial organization of large structures in the turbulent far wake of a cylinder. *J. Fluid Mech.* **218**, 439–461.

BUDNY, R. S., KAWALL, J. G. & KEFFER, J. F. 1979 Vortex street evolution in the wake of a circular cylinder. *Second Symp. on Turbulent Shear Flows, Imperial College*, pp. 7.20–7.25.

DAVIES, M. E. 1976 A comparison of the wake structure of a stationary and oscillating bluff body, using a conditional averaging technique. *J. Fluid Mech.* **75**, 209–231.

ELLIOT, C. J. & TOWNSEND, A. A. 1981 The development of a turbulent wake in a distorting duct. *J. Fluid Mech.* **113**, 433–467.

FERRÉ, J. A. & GIRALT, F. 1989*a* Pattern-recognition analysis of the velocity field in plane turbulent wakes. *J. Fluid Mech.* **198**, 27–64.

FERRÉ, J. A. & GIRALT, F. 1989*b* Some topological features of the entrainment process in a heated turbulent wake. *J. Fluid Mech.* **198**, 65–78.

FERRÉ, J. A., MUMFORD, J. C., SAVILL, A. M. & GIRALT, F. 1990 Three-dimensional large-eddy motions and fine-scale activity in a plane turbulent wake. *J. Fluid Mech.* **210**, 371–414.

GIRALT, F. & FERRÉ, J. A. 1993 Structure and flow patterns in turbulent wakes. *Phys. Fluids* A **5**, 1783–1789.

GRANT, H. L. 1958 The large eddies of turbulent motion. *J. Fluid Mech.* **4**, 149–190.

HUANG, Z., FERRÉ, J. A., KAWALL, J. G. & KEFFER, J. F. 1993 The evolution of coherent structures in the plane turbulent wake of a porous body. *3rd World Conf. on Exp. Heat Transfer, Fluid Mech. and Thermodynamics, Honolulu*, pp. 1001–1108.

HUNT, J. C. R. & MULHEARN, P. J. 1973 Turbulent dispersion from sources near two-dimensional obstacles. *J. Fluid Mech.* **61**, 245–274.

KAWALL, J. G. & KEFFER, J. F. 1982 The role of coherent structures in the development of a uniformly strained turbulent wake. *Turbulent Shear Flows 3* (ed. L. J. S. Bradbury *et al.*), pp. 132–145. Springer.

KEFFER, J. F. 1965 The uniform distortion of a turbulent wake. *J. Fluid Mech.* **22**, 135–159.

KEFFER, J. F., KAWALL, J. G., HUNT, J. C. R. & MAXEY, M. R. 1978 The uniform distortion of thermal and velocity mixing layers. *J. Fluid Mech.* **86**, 465–490.

KOPP, G. A., KAWALL, J. G. & KEFFER, J. F. 1995 A diagnostic experimental technique for studying coherent structures in plane turbulent wakes. In *Flow Measurement and Instrumentation*, vol. 6 (in press).

LAMB, H. 1932 *Hydrodynamics*. Cambridge University Press.

REYNOLDS, A. J. 1962 Observations on distorted turbulent wakes. *J. Fluid Mech.* **13**, 333–355.

TAYLOR, G. I. 1935 Turbulence in a contracting stream. *Z. Angew. Math. Mech.* **15**, 91–96.

TOWNSEND, A. A. 1954 The uniform distortion of homogeneous turbulence. *Q. J. Mech. App. Maths* **7**, 104–127.

TOWNSEND, A. A. 1966 The mechanism of entrainment in free turbulent flows. *J. Fluid Mech.* **26**, 689–715.

TOWNSEND, A. A. 1970 Entrainment and the structure of turbulent flow. *J. Fluid Mech.* **41**, 13–46.

TOWNSEND, A. A. 1980 The response of shared turbulence to additional distortion. *J. Fluid Mech.* **81**, 171–91.

TUCKER, H. J. & REYNOLDS, A. J. 1968 The distortion of turbulence by irrotational plane strain. *J. Fluid Mech.* **32**, 657–673.